Microstructure of $SiO_2-Al_2O_3-CaO-P_2O_5-K_2O-F^-$ Glass Ceramics. 1. Needlelike versus Isometric Morphology of Apatite Crystals

Thomas Höche,* Cornelia Moisescu, Issak Avramov,† and Christian Rüssel

Otto-Schott-Institut für Glaschemie, Friedrich-Schiller-Universität, Fraunhoferstrasse 6, D-07743 Jena, Germany

Wolfgang D. Heerdegen

Institut für Optik und Quantenelektronik, Friedrich-Schiller-Universität Jena, Max-Wien-Platz 1, D-07743 Jena, Germany

Received October 17, 2000. Revised Manuscript Received January 8, 2001

In $SiO_2-Al_2O_3-CaO-P_2O_5-K_2O-F^-$ glasses, either spherical or needlelike fluorapatite crystals can be formed depending on the heat-treatment schedule. If the annealing is performed at 800 °C or low heating rates are applied, isometric apatite crystallizes whereas the heat treatment at 1200 °C in conjunction with high heating rates results in apatite needles. On the basis of the combination of ^{31}P MAS NMR spectrometry, transmission-electron microscopic imaging, and energy-dispersive X-ray spectrometry, a crystallization model capable of explaining the morphology change is derived. Phase-separation processes are shown to have a major impact on the composition of the residual glass hosting apatite crystals and the structure and composition of the glass matrix in turn determine the fluorapatite morphology observed. At 800 °C, spherical crystals are formed since the two different growth modes parallel and perpendicular to the crystallographic *c* axis of apatite (provoking anisometric growth at high temperature) are outweighed by hampered diffusion.

1. Introduction

The principal inorganic component of the hard tissue is closely related to the basic calcium phosphate, $Ca_{10}(PO_4)_6(OH)_2$, hydroxyapatite. For both bone implants and restorative dentistry applications, various glass-ceramic materials have been developed over the past 25 years. Glass-ceramics (GCs) bone substitutes can be subdivided into two groups: the apatite-wollastonite GCs developed by Kokubo et al.[1] and mica-based materials originally synthesized by Beall[2] and later also by Vogel and Höland.[3] In restorative dentistry, GCs are mainly based on glasses precipitating apatite.[1] As opposed to mineralized tissue containing oriented elongated apatite crystals, the morphology of apatite crystals in the early synthetic materials used to be isometric and it was only later that GCs containing apatite needles were developed.[4−7]

Recently, Moisescu et al.[8] prepared single-crystalline-phase GCs containing apatite needles from a $SiO_2-Al_2O_3-CaO-P_2O_5-K_2O-F^-$ glass using high heating rates and a crystallization temperature of 1200 °C. After apatite needles were grain-oriented by post-crystallization extrusion,[9] those GCs exhibited an enhanced fracture toughness, K_{Ic}.[10] This finding parallels the behavior observed with grain-oriented lithium disilicate GCs[11] and mica GCs[12−15] since K_{Ic} perpendicular to the extrusion direction (1.46 $MPa \cdot m^{-1/2}$) is improved on the expense of K_{Ic} parallel to the direction of extrusion (0.9 $MPa \cdot m^{-1/2}$).

Texturing by extrusion is most efficient for crystalline phases with well-expressed anisometry. Therefore, the present contribution focuses on the growth mechanisms

* To whom correspondence should be addressed. Fax: +49 3641 948 502. E-mail: hoeche@glas.chemie.uni-jena.de. Current address: Lehrstuhl für Kristallographie, Institut für Physik, Humboldt-Universität zu Berlin, Invalidenstrasse 110, D-10115 Berlin, Germany.

† On leave from the Institute for Physical Chemistry, Bulgarian Academy of Sciences, 1113 Sofia, Bulgaria.

(1) Kokubo, T.; Shigematsu, M.; Hagashima, Y.; Tashiro, T.; Nakaura, T.; Yamamuro, T.; Higashi, H. *Bull. Inst. Chem. Red. Kyoto Univ.* **1982**, *30*, 260.

(2) Beall, G. H.; Chyung, K.; Watkins, H. J. *Fluormica Glass-Ceramics*; U.S. Patent US-PS 3,801,295, Apr. 2, 1974.

(3) Vogel, W.; Höland, W.; Naumann, K.; Gummel, J. *J. Non-Cryst. Solids* **1986**, *80*, 34.

(4) Avery, J. K. *Oral Development and Histology*, 2nd ed.; Thieme Medical Publishers: New York, 1994.

(5) Hill, R.; Wood, D. *J. Mater. Sci.: Mater. Med.* **1995**, *6*, 311.

(6) Höland, W.; Frank, M.; Schweiger, M.; Rheinberger, V. *Glastech. Ber. Glass Sci. Technol.* **1994**, *67C*, 117.

(7) Müller, R.; Abu-Hilal, L. A.; Reinsch, S.; Höland, W. *J. Mater. Sci.* **1999**, *34*, 65.

(8) Moisescu, C.; Jana, C.; Rüssel, C. *J. Non-Cryst. Solids* **1999**, *248*, 169.

(9) Moisescu, C.; Jana, C.; Habelitz, S.; Carl, G.; Rüssel, C. *J. Non-Cryst. Solids* **1999**, *248*, 176.

(10) Moisescu, C.; Jana, C.; Carl, G.; Habelitz, S.; Rüssel, C. *Glastech. Ber. Glass Sci. Technol.* **1998**, *71C*, 150.

(11) Durschang, B. R.; Carl, G.; Rüssel, C.; Marchetti, K.; Roeder, E. *Glastech. Ber. Glass Sci. Technol.* **1994**, *67*, 171.

(12) Habelitz, S.; Carl, G.; Rüssel, C.; Marchetti, K.; Roeder, E.; Eifler, D.; Hergt, R. *Glastech. Ber. Glass Sci. Technol.* **1997**, *70*, 86.

(13) Höche, T.; Habelitz, S.; Khodos, I. I. *J. Cryst. Growth* **1998**, *192*, 185.

(14) Höche, T.; Habelitz, S.; Avramov, I. *Acta Mater.* **1999**, *47*, 735.

(15) Habelitz, S.; Höche, T.; Hergt, R.; Carl, G.; Rüssel, C. *Acta Mater.* **1999**, *47*, 2831.

10.1021/cm001203p CCC: $20.00
Published on Web 03/14/2001

Table 1. Overall Composition of the Basic Glass Determined by Electron Probe Microanalysis (Be-Window) in a Scanning Electron Microscope [Averaging over a Large Area (50 × 50 μm^2), Fluorine Content Wet-Chemically Analyzed]

mol % Na_2O	mol % Al_2O_3	mol % SiO_2	mol % P_2O_5	mol % K_2O	mol % CaO	mol % F^-
0.5	23.5	9.5	26.2	6.8	16.4	8.1

Table 2. Specimens and Their Heat-Treatment Schedules

specimen	preparation of the glass	heat treatment	extrusion at 700 °C (∼30 min)
A	quenching at ≈350 K·s^{-1}	no further treatment	no
B	casting (≈20 K·s^{-1})	no further treatment	no
C	casting	800 °C for 2 min	no
D	casting	800 °C for 5 min	no
E	casting	800 °C for 30 min	no
F	casting	1200 °C for 2 min	no
G	casting	1200 °C for 30 min	yes

by which in the same glass—depending on the thermal treatment—apatite crystals either grow isometric or are needlelike-shaped. The growth model presented here is based on experiments combining ^{31}P MAS NMR, electron microscopic imaging, selected-area electron diffraction, and energy-dispersive X-ray spectrometry in the transmission electron microscope and X-ray powder diffraction. The time dependence of the apatite growth is detailed in the companion article.[16]

2. Experimental Section

2.1. Preparation of Apatite Glass Ceramics. A SiO_2–Al_2O_3–CaO–P_2O_5–K_2O–F^- glass (Table 1) was prepared by melting SiO_2 (quartz), K_2CO_3, $CaCO_3$, $Al(PO_3)_3$, K_3AlF_6, and $AlOOH \cdot H_2O$ in an Al_2O_3 crucible inside an electrically heated furnace. The glass melt was poured into water and remelted in a platinum crucible at 1500–1550 °C for 1 h. Finally, the glass was either casted in graphite moulds or quenched between a pair of cooled steel rollers.

Crystallization of the glass was performed by annealing at 800 or 1200 °C after millimeter-sized samples were inserted into the preheated furnace (heating rate: ≈20 K·s^{-1}). For all samples, the method of cooling (casting or quenching), the subsequent thermal treatment, and the respective notation are summarized in Table 2.

The extrusion of heat-treated samples is described in the companion article.[16]

2.2. Microstructural Characterization. The phosphorus distribution among different microstructural constituents present in glasses and glass ceramics was determined by ^{31}P magic-angle spinning nuclear magnetic resonance (MAS NMR) spectrometry at 162 MHz (BRUKER AMX 400, MAS spinning frequency: 14 kHz, chemical shifts referenced to 85% H_3PO_4). Since the prior intention of the measurements was to determine the relative content of different phases in the samples, the repetition time of the experiment had to be as long as the longest relaxation time of all phases (600 s).

The assignment of spectral features in the ^{31}P MAS NMR spectra was established by careful comparison with corresponding X-ray powder diffraction data (Siemens diffractometer D5000, 2θ range: 10°–50°, Cu Kα radiation), TEM diffraction patterns, and TEM images of the microstructure.

In X-ray powder diffraction, two constraints apply: (i) crystalline phases with a volume fraction smaller than about 5% cannot be discerned, and (ii) the discrimination between fluorapatite, hydroxyapatite, tricalciumphosphate, and tetracalciumphosphate on the basis of X-ray diffractograms is hardly possible. In contrast, ^{31}P MAS NMR in conjunction with ^{17}F MAS NMR is capable of discriminating between the alternatives.[17,18] For this reason, X-ray data are not explicitly shown here, although they are used for understanding the microstructural evolution.

The composition of microstructural constituents was analyzed with high spatial resolution by energy-dispersive X-ray spectrometry (EDXS, Si:Li detector, atmospheric thin window) in a transmission electron microscope (Hitachi H-8100 II, 200 kV acceleration voltage, LaB_6 filament). Elemental concentrations from TEM EDXS analyses presented here are based on the determination of element ratios (for elements with atomic number larger than 11) using experimental Cliff–Lorimer factors. Those ratios were normalized to 100% after stoichiometric addition of oxygen and fluorine (the F^- content was determined via the experimentally determined O:F ratio).

Samples for TEM analyses were prepared by cutting slices, plane-parallel grinding, dimpling to a residual thickness of 10–15 μm, and ion-beam thinning using Ar^+ ions. By means of double-sided ion-beam etching at small angles (<6°) and low etching energies (acceleration voltage: 2.5 kV; beam current < 1.5 mA), substantial heating of the TEM foils and consequently the introduction of artifacts were avoided.

The morphological characterization of respective phases in glasses and glass ceramics mainly rests on the imaging of replica films in the TEM. The latter films were prepared as detailed in ref 19 from chemically etched glasses (1:1 mixture of 2.5% HF and 2.5% HNO_3 applied for 2 s). For longer annealing times (i.e., larger FAp crystals), replica films tended to crack and thus the replica method was completed by imaging of identically etched samples in a scanning electron microscope (Zeiss DSM 940 A).

3. Results and Discussion

3.1. Characterization of the SiO_2–Al_2O_3–CaO–P_2O_5–K_2O–F^- Glass. The glass investigated is subject to liquid–liquid phase separation and the TEM replica micrograph of the rapidly quenched sample A (cooling rate ≈ 350 K·s^{-1}, Figure 1a) illustrates that liquid–liquid phase-separation droplets (PSDs) with an average diameter of about 50 nm are embedded in a glassy matrix. There is no indication of any crystalline phase after quenching by either of the applied methods.

Upon casting of the glass (cooling rate ∼ 0.3 K·s^{-1}, Figure 1b), a coarsening of the droplets to an average size of ca. 500 nm occurs. Moreover, about half of the PSDs is converted into crystalline Fluorapatite (FAp) as proved by X-ray powder diffraction and electron diffraction and illustrated by Figure 1c.

Speckles to be seen inside FAp crystals in Figure 1c correspond to inclusions which are either amorphous or crystalline. These inclusions indicate another (secondary) liquid–liquid phase separation taking place inside the large (primary) PSDs. The crystalline $AlPO_4$ inclusion marked by the arrow in Figure 1c proves not only that fluorapatite does not necessarily crystallize first but also that secondary PSDs can crystallize inside a still amorphous primary droplet. The fact that primary PSDs appear unstructured in TEM micrographs recorded from transmission samples must be attributed to the combined effect of the very small size of secondary

(16) Höche, T.; Moisescu, C.; Avramov, I.; Rüssel, C.; Heerdegen, W. D.; Jäger, C. *Chem. Mater.* **2001**, *13*, 1320.

(17) Braun, M.; Jana, C. *Chem. Phys. Lett.* **1995**, *245*, 19.

(18) Heerdegen, W. D.; Braun, M.; Jana, C.; Moisescu, C.; Jäger, C.; Rüssel, C. *Glastech. Ber. Glass Sci. Technol.* **1998**, *71C*, 309.

(19) Vogel, W.; Horn, L.; Völksch, G. *J. Non-Cryst. Solids* **1982**, *49*, 221.

(20) Rothwell, W. P.; Waugh, J. S.; Yesinowski, J. P. *J. Am. Chem. Soc.* **1980**, *102*, 2637.

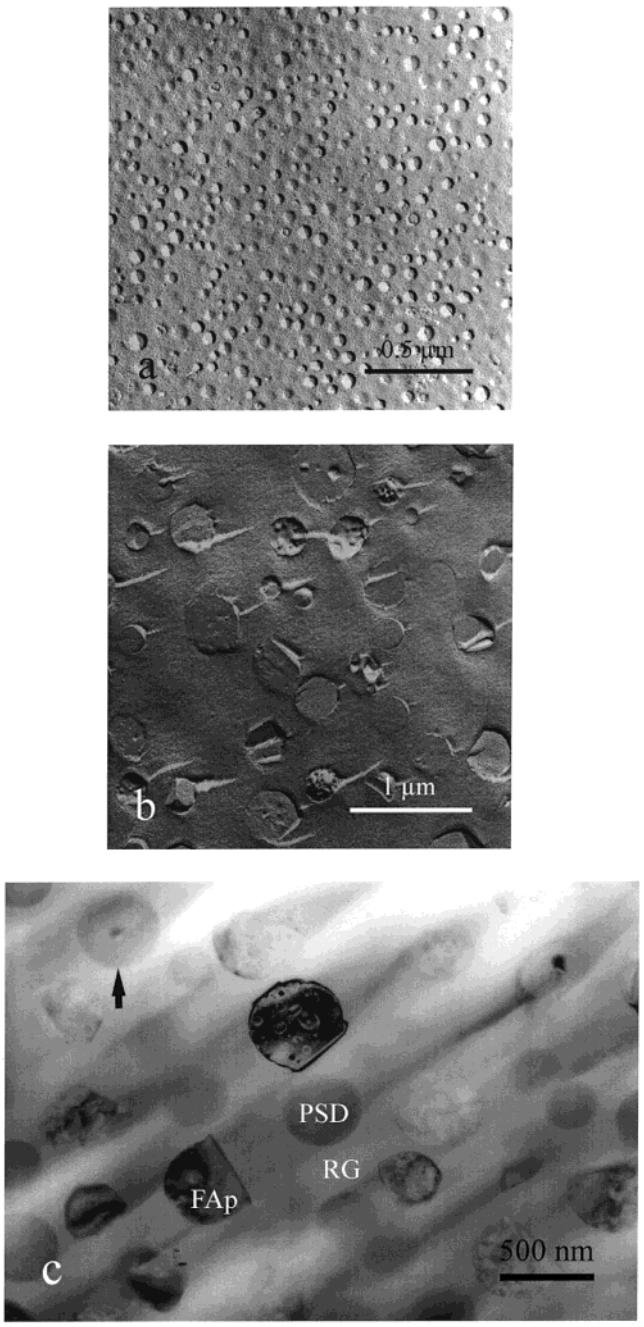

Figure 1. TEM replica micrographs of (a) the quenched sample A and (b) the as-cast sample B. (c) TEM overview of the as-cast glass (transmission sample B). Nonstructured spherical regions corresponding to phase separation droplets (PSDs) and speckled fluorapatite crystals (FAp) containing a large number of several 10 nm large inclusions are embedded in the residual glass (RG).

PSDs (10−100 nm diameter) and the absence of a significant difference in the average atomic number of primary and secondary PSDs.

Since the casted sample B represents the initial state all subsequent heat treatments do start from, the chemical composition of all constituents of the microstructure was determined by means of TEM-EDXS analysis. It turned out (cf. Table 3) that in comparison to the residual glass, primary phase separation droplets are significantly enriched in fluorine, phosphorus, and calcium while the aluminum and silicon content is drastically reduced. It must be noted that the TEM-EDXS analysis of primary PSDs concerns *entire* droplets including secondary PSDs hosted by the primary PSDs. Consequently, the composition of PSDs given in Table 3 should be regarded as a weighted average over primary and secondary PSDs. If primary PSDs are converted into FAp, however, easily visible inclusions are formed, which can be investigated by TEM-EDXS. Although these inclusions suffer from severe radiation damage and their sizes range between 10 and 100 nm only, EDXS analysis indicates the existence of at least two different types of glassy inclusions (Table 3). Both types of inclusions, however, exhibit twice as high aluminum content in comparison to that of the spectra acquired from (whole) primary PSDs. The trapping of aluminum in the secondary PSDs (primary PSDs are assumed to be virtually free of Al) facilitates FAp crystallization since aluminum cannot be incorporated in the FAp lattice. As mentioned above, some fraction of the secondary PSDs can also crystallize and form $AlPO_4$ (presumably, from phosphorus-rich secondary PSDs of type I, Table 3).

^{31}P MAS NMR spectra can be interpreted in terms of linkage between PO_4 tetrahedra. But a necessary prerequisite for such an interpretation is the attribution of spectral features to microstructural equivalents. With a comparison of numerous ^{31}P MAS NMR spectra with corresponding X-ray powder diffraction patterns and images recorded in the TEM, the following assignments were made (compare Figure 2): The very sharp peak at a chemical shift (CS) of +2.2 ppm corresponds to crystalline FAp.[20,21] Although the origin of the pre- and postpeak shoulder of the apatite peak could not be finally clarified, according to Braun,[22] a correspondence to tetracalcium diphosphate monoxide, $Ca_4(PO_4)_2O$ seems to be most likely. In the casted glass, in addition to the very sharp apatite maximum, there are two broad peaks centered at CS = −5.4 ppm and CS = −23.4 ppm. Since the latter peak persists upon subsequent heat treatments (i.e., upon the dissolution of primary PSDs), it is assigned to the glassy matrix and the peak at CS = −5.4 ppm is attributed to primary PSDs. The CS of the primary-PSD peak clearly shows that the vast majority of PO_4 tetrahedra in the large primary droplets forms Q^0 and Q^1 groups; that is, there are mainly isolated PO_4 groups and the tendency to form a network is low. In contrast, in the glass matrix, Q^2 groups dominate; that is, PO_4 tetrahedra are forming long, mainly linear, chains. Those connectivity assignments imply that the crystallization of FAp within Q^0 and Q^1-dominated primary PSDs is facilitated since only a small number of bonds have to be rearranged to convert the glass into FAp.

In conclusion, of the last two paragraphs, both the composition of and the connectivity within large, primary PSDs highly facilitate the crystallization of fluorapatite. Consequently, the growth rate of FAp inside primary PSDs is very high (primary PSDs only partly converted into FAp could never be observed).

(21) Braun, M.; Hartmann, P.; Jana, C. *J. Mater. Sci. Mater. Med.* **1995**, *6*, 150.

(22) Braun, M. *Aufbau einer Anordnung zur kernmagnetischen Doppelresonanz der Kernkombination ^{31}P-^{19}F/^{1}H bei B_0=6, 35 T und deren Anwendung zu Strukturuntersuchungen an Hexafluorophosphaten und Apatiten*; Ph.D. Thesis, Friedrich-Schiller-University Jena, 1994.

Table 3. TEM EDXS Data [Note that Error Bars (Standard Errors) Given in the Last Line Are Calculated from the Statistical Scattering of Data, That is, Systematic Errors Are Not Included]

sample	phase	mol % O	mol % F	mol % Na	mol % Al	mol % Si	mol % P	mol % K	mol % Ca
stoichiometric fluorapatite		57.1	4.8				14.3		23.8
B	PSD	50.04	18.37	0.26	5.22	1.56	9.71	0.56	14.27
B	inclusion I	54.6	18.0	0.3	11.1	1.4	13.9	0.6	
B	inclusion II	57.8	11.2	0.7	11.5	11.5	6.6	0.7	
B	glass	56.38	10.25	0.67	10.75	13.8	3.81	3.76	0.57
C	glass	59.05	6.13	0.91	11.79	13.66	4.48	3.20	0.77
D	glass	55.08	10.96	1.29	12.18	10.63	4.82	4.36	0.69
E	glass	54.98	11.14	1.61	11.34	12.83	3.55	3.84	0.70
F	glass	55.16	10.03	1.51	11.3	11.47	4.03	5.66	0.84
G	glass	55.23	10.04	0.85	12.1	11.59	3.8	5.67	0.72
average error (glass)		±2%	±8%	±10%	±5%	±3%	±5%	±10%	±7%

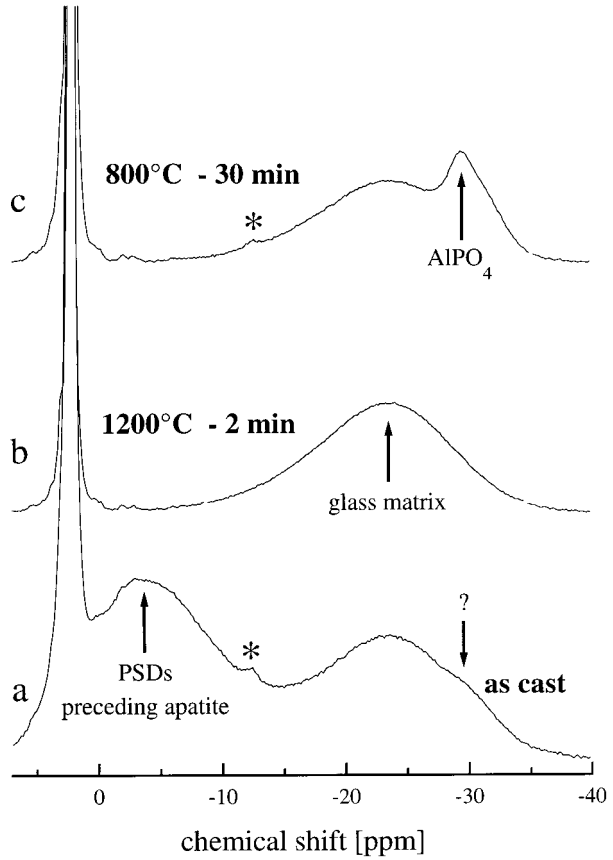

Figure 2. ^{31}P MAS NMR spectra of (a) the cast glass and glass ceramics heat-treated at (b) 1200 °C for 2 min and (c) 800 °C for 30 min. The tiny peaks marked by asterisks are rotor artifacts (during highly sensitive measurements some phosphorus-containing compound "implanted" into the rotor did contribute to the overall signal as proved by acquiring data from a pure Teflon sample). The interpretation of the shoulder in the lower spectrum marked by "?" is given in the text.

In addition to the above-mentioned information on PO_4 tetrahedra linkage, the distribution of phosphorus among the constituents of the microstructure can also be determined from ^{31}P MAS NMR spectra. As compiled in Table 4, in sample A (quenched), 65% of the phosphorus is located in PSDs and the remaining 35% P is hosted by the residual glass. In the casted sample B, however, the amount of phosphorus in PSDs has become reduced to one-third. Since the P content in the glass matrix remains almost constant, it can be concluded that only very few PSDs were dissolved in the ambient glass matrix upon casting and the "missing" PSDs were converted into crystalline FAp.

Recalling compositional differences between glassy matrix, PSDs, and FAp crystals, it is desirable to convert the distribution of phosphorus into molar fractions of the corresponding phases. Denoting the phosphorus content determined by NMR spectroscopy by P_P and the molar fraction of phosphorus from TEM-EDXS by c_P, the ratio of the aforementioned, x_i, for the microstructural constituent i becomes

$$x_i = \frac{P_P^i}{c_P^i} \tag{1}$$

Thus, the molar fraction of phase i, X_i, is given by

$$X_i = \frac{x_i}{\sum_{\text{all phases}} x_i} \tag{2}$$

In particular, for a sample containing two phases (e.g., glassy matrix and one crystalline phase), the degree of crystallization, α, reads like

$$\alpha = \frac{X_{\text{crystal}}}{X_{\text{matrix}} + X_{\text{crystal}}} \tag{3}$$

In the case of FAp crystals being embedded in a homogeneous glass, α becomes

$$\alpha = \frac{P_P^{\text{apatite}} c_P^{\text{glass}}}{0.143(1 - P_P^{\text{apatite}}) + P_P^{\text{apatite}} c_P^{\text{glass}}} \tag{4}$$

where the superscripts refer to the corresponding phases and the phosphorus concentration in FAp was replaced by the nominal value for stoichiometric FAp (14.3%). In addition to the raw data of the phosphorus distribution, molar fractions of all NMR-detectable phases are compiled in Table 4. Secondary PSDs (glassy or crystalline) cannot be detected because of their very minor amounts.

3.2. Heat Treatment at 1200 °C. The heat treatment of the cast glass at 1200 °C results in the formation of FAp needles unless heating rates are kept very low. When high heating rates (20 $K \cdot s^{-1}$) are used, already after 2 min at 1200 °C, an average needle length of about 1 μm is observed at an aspect ratio of 2:1 (Figure 3a). After 30 min at 1200 °C (Figure 3b), the average length has increased to 2.5 μm with an aspect ratio of 4:1.[23] As evidenced by TEM imaging (Figure 3a) and ^{31}P MAS NMR spectroscopy (Figure 2b), primary PSDs are no longer existent after a 2-min long heat

Table 4. ^{31}P MAS NMR Results on the Phosphorus Distribution among Microstructural Constituents Together with the Molar Fraction Calculated from These Data

sample	remarks	phosphorus in PSDs [atom %]	phosphorus in glass matrix [atom %]	phosphorus in apatite [atom %]	phosphorus in $AlPO_4$ [atom %]	molar fraction PSDs [%]	molar fraction glass matrix [%]	molar fraction FAp [%]	molar fraction $AlPO_{4\,[\%]}$
A	quenched glass	65 ± 5	35 ± 5			42 ± 6	58 ± 6		
B	cast glass	24 ± 2	37 ± 2	39 ± 2		17 ± 2	65 ± 6	18 ± 2	
C	800 °C, 2 min	26 ± 2	39 ± 2	35 ± 2		19 ± 2	63 ± 6	18 ± 2	
D	800 °C, 5 min		44 ± 2	56 ± 2			70 ± 7	30 ± 3	
E	800 °C, 30 min		34 ± 2	58 ± 2	8 ± 2		63 ± 6	33 ± 3	4 ± 1
F	1200 °C, 2 min		46 ± 2	54 ± 2			76 ± 8	24 ± 2	

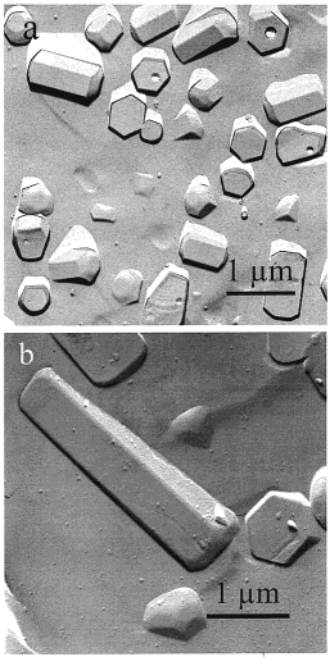

Figure 3. TEM micrographs of samples heat-treated at 1200 °C for (a) 2 min and (b) 30 min.

treatment at 1200 °C. According to molar fractions calculated from ^{31}P MAS NMR and EDXS data (Table 4), already after 2 min at 1200 °C, about one-third of the PSDs not yet crystallized upon casting (sample B) becomes FAp crystals and the remaining two-thirds is dissolved in the matrix glass. This dissolution is accompanied by an increase in the Ca, P, and Al contents in the glassy matrix as shown in Figures 4a−c. However, within <30 min at 1200 °C this surplus in the calcium and phosphorus content is consumed by the growing apatite crystal and equilibrium values are adjusted. Within the first few minutes, the higher Ca and P content raises the supersaturation and in turn the linear growth rate along the needle axis, v_z, is high (between 2 and 3 nm/s). After equilibrium values of element concentrations have been adjusted (≥30 min at 1200 °C), v_z drops by an order of magnitude—for details of FAp needle growth, see the companion article.[16]

3.3. Heat Treatment at 800 °C. In contrast to the findings at 1200 °C, after 2 min of annealing at 800 °C, primary PSDs are still present (Figure 5a), and according to ^{31}P MAS NMR data, the molar fraction of primary PSDs even does not change with respect to the cast glass within the experimental error.

(23) A detailed account of the time dependence of the needle length observed after thermal treatment at 1200 °C is given in the companion article (ref 16).

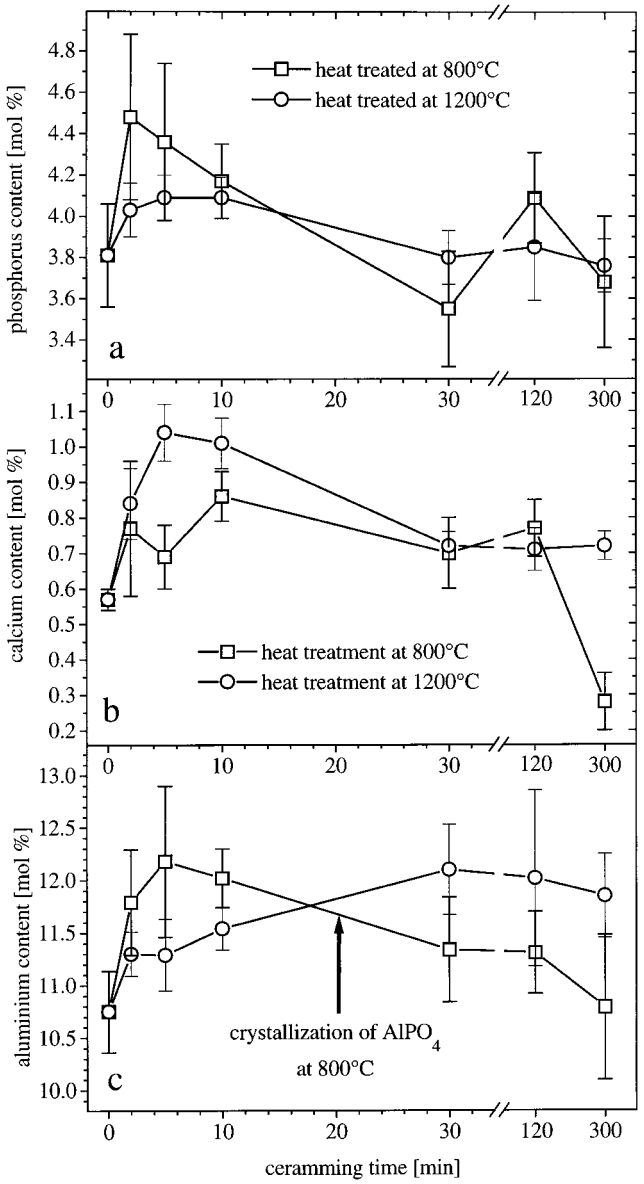

Figure 4. Time dependence of the P, Ca, and Al concentration in the residual glass determined by EDXS after heat treatment at 800 and 1200 °C, respectively. For each data point, between 8 and 10 independent EDXS analyses were averaged. Error bars given correspond to the mean error of the average value. Note the unconventional axis increment after the abscissa break. Connecting lines are intended to serve as guides to the eye.

However, after being exposed to 800 °C for 5 min (Figure 5b), primary PSDs have disappeared and in comparison to sample F (1200 °C, 2 min), the molar fraction of FAp crystals is about 25% higher, indicating that a significantly larger number of primary PSDs

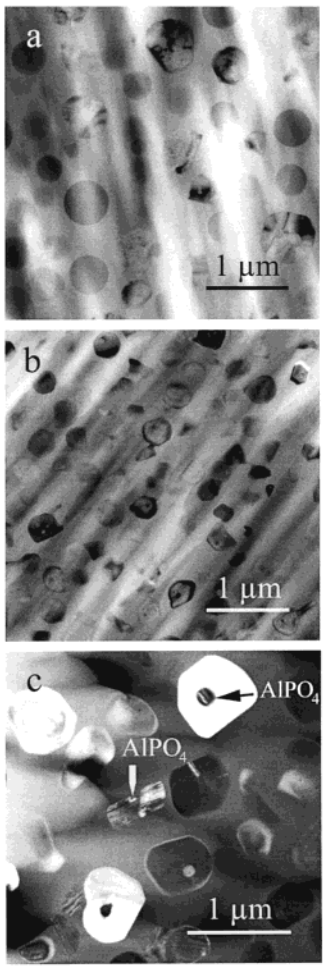

Figure 5. TEM micrographs of samples heat-treated at 800 °C for (a) 2 min, (b) 5 min, and (c) 30 min.

becomes crystallized. Figure 5c illustrates that the size of the isometric FAp crystals does not exceed 800 nm after 30 min, and even after 5 h, the average size remains at ≈800 nm.[16]

Although less PSDs dissolve at 800 °C in comparison to those in the 1200 °C heat treatment, also here, the glass matrix becomes enriched in Ca and P (open squares in Figure 4a,b). However, contrary to the thermal treatment at 1200 °C, after 30 min at 800 °C, the formation of highly defective $AlPO_4$ crystals is observed. The analysis of the respective ^{31}P MAS NMR spectrum (Figure 2c) reveals an additional peak at CS = − 29.4 ppm, which can be assigned to $AlPO_4$ in the tridymite modification.[24] While chemical shifts, indicative of the bonding through the linkage between PO_4 tetrahedra, are not affected by the extremely large number of stacking faults visible in Figure 6, the peak broadening can be correlated to the observed defectiveness of the tridymite structure.

3.4. Ceramming Mechanism. At 800 °C, a 25% higher volume fraction of primary PSDs crystallize into FAp in comparison to the heat treatment at 1200 °C (samples D and F in Table 4). Recalling the chemical composition of PSDs (Table 3), it is evident that the dissolution of PSDs will significantly increase the Ca, P, and F content in the surrounding glass matrix and exactly this behavior is found for both heat treatments (Figure 4). The enrichment in calcium, phosphorus, and fluorine in turn increases the supersaturation driving the crystallization of FAp and consequently crystal growth rates are rather high under the conditions of high supersaturation. Upon consumption of the FAp-constituting elements calcium, phosphorus, and fluorine, however, the composition of the glass matrix is adjusted at an equilibrium resulting in a decrease of both the supersaturation and the growth rate within 30 min.

But why is the FAp crystal morphology obtained at 800 °C so completely different from that found at 1200 °C? The answer will be given in the following referring to the schematic drawing shown in Figure 7.

First of all, it must be concluded that the decision as to which morphology will be adopted is made within the first few minutes since Figures 3a and 5b show that the difference between samples heat treated at either 1200 or 800 °C does exist immediately after all PSDs are dissolved. Thus, the chemical composition of the matrix glass at these stages (samples D and F) must be considered. The close inspection of Figure 4 reveals the following:

(i) The *phosphorus content* in the glass matrix is about 10% higher at 800 °C in comparison to the 1200 °C value. This finding is unexpected since the dissolution of a larger volume fraction of PSDs at 1200 °C would imply that also the phosphorus content should be higher than that at 800 °C. But the discrepancy can be explained assuming that the phosphorus distribution in the glass matrix is *not homogeneous* at 800 °C. Recalling the fact that, after 30 min at 800 °C, crystalline $AlPO_4$ is formed, it is reasonable to propose that the crystallization process is preceded by some agglomeration of aluminum and PO_4 groups. In fact, there is clear experimental evidence for such a miscibility gap facilitating the crystallization of $AlPO_4$ in a very similar but aluminum-enriched and less calcium-containing glass (32.4 mol % Al_2O_3, 21.4 mol % SiO_2, 19.6 mol % P_2O_5, 8.3 mol % K_2O, 9.9 mol % CaO, 8.4 mol % F^-, cf. Figure 8).[25] For the glass considered up to now, such agglomeration of aluminum and phosphorus would explain the measured increasing phosphorus content in the residual glass after thermal treatment at 800 °C in comparison to the annealing at 1200 °C: since electron-beam spots were placed well between FAp crystals (to avoid overlap with FAp), they have fitted the most probable regions for Al and P enrichment. Returning to the ^{31}P NMR spectrum of the cast sample (Figure 2a), there is the indication of a shoulder located at the glass-matrix broad maximum at CS ca. −30 ppm. Although such a value of CS might also correspond to some calcium phosphate or potassium phosphate, it is reasonable to assume that it originates from the aluminum- and phosphorus-enriched areas between FAp crystals as the CS conicides with that for $AlPO_4$ (tridymite), Figure 2c. In this context, two-dimensional NMR experiments[26] are planned to gain a deeper insight into the glass structure in terms of connectivity.

(24) Müller, D.; Jahn, E.; Ladwig, G.; Haubenreisser, U. *Chem. Phys. Lett.* **1984**, *109*, 332.

(25) In this system, upon heat treatment at 900 °C $AlPO_4$ is found to predominantly crystallize in well-defined, droplet-like regions of 5−10 μm diameter that are surrounded by apatite-containing glass of different compositions. If the same glass is heat-treated at 1200 °C, no $AlPO_4$ is observed.

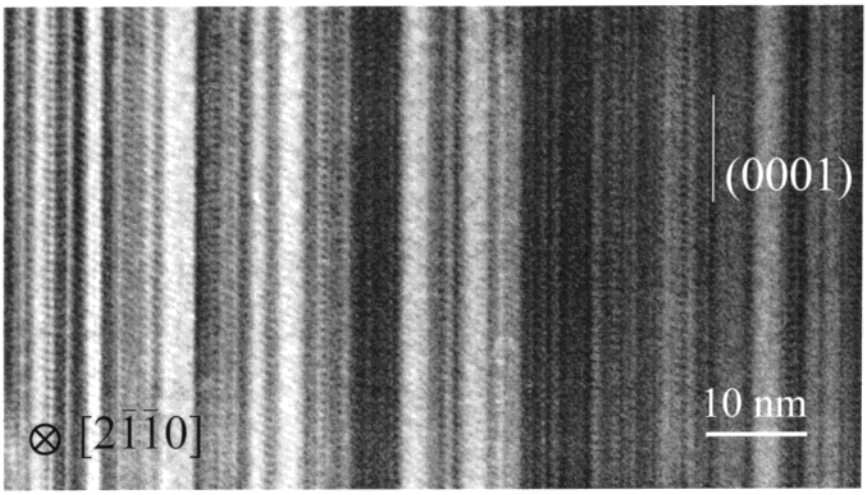

Figure 6. Lattice-plane image of the highly defective $AlPO_4$. Whenever observed in the glass ceramics reported here, tridymite $AlPO_4$ did contain stacking faults perpendicular to the (0001) plane occurring in disordered sequences.

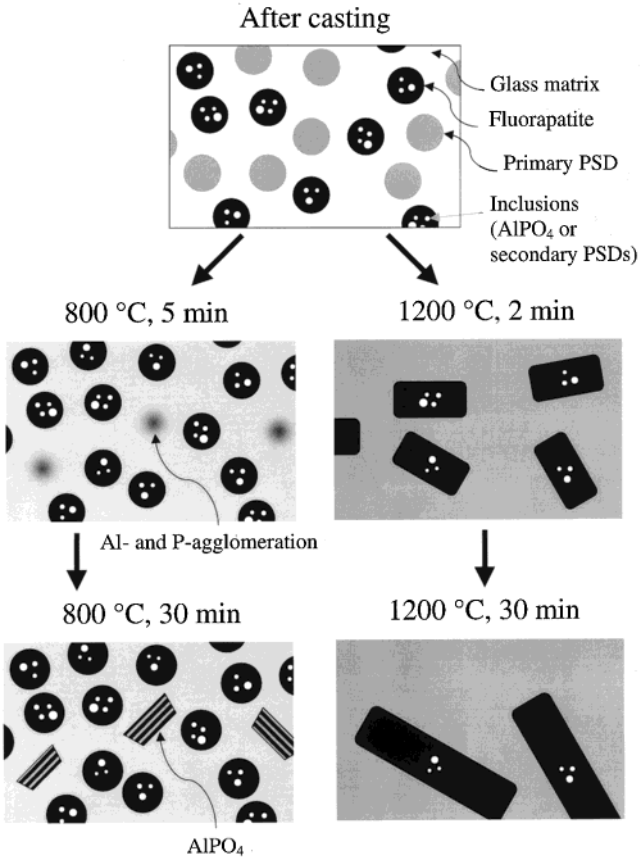

Figure 7. Ceramming scheme for heat treatments at 800 and 1200 °C.

(ii) The above idea of an agglomeration is well-supported by the time dependence of the *aluminum content* at 800 and 1200 °C since also here, an obvious enrichment of aluminum within the first 10 minutes at 800 °C is observed. Later on, the aluminum content is clearly reduced upon the formation of $AlPO_4$ after 30 min at 800 °C.

(26) Jäger, C. Two-Dimensional NMR Investigation of the Structure of Glasses: Novel Approaches. In *Analysis of the Composition and Structure of Glass and Glass Ceramics*; Bach, H., Krause, D., Eds.; Springer-Verlag: Berlin, 1999; p 207.

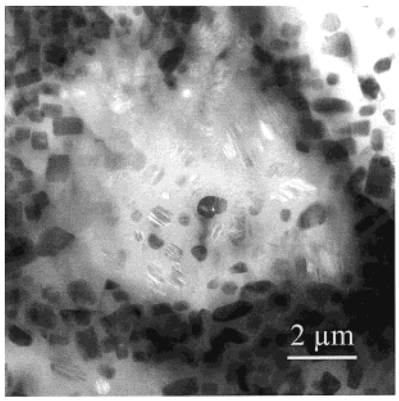

Figure 8. TEM micrograph of a glass containing more aluminum and less calcium after heat treatment for 1 h at 900 °C. Within bright, glassy regions of the glass, $AlPO_4$ crystals can be clearly identified because of their high density of stacking faults whereas the surrounding (less bright) glass matrix contains FAp crystals only.

(iii) The *calcium concentration* behaves in the "expected" manner since the calcium content within the first 30 min is about 20% higher at 1200 °C in comparison with the samples heat treated at 800 °C.

Summarizing the above-mentioned data, the formation of aluminum- and phosphorus-enriched regions *between* FAp crystals at 800 °C (as a preliminary stage of the crystallization of $AlPO_4$) removes significant amounts of phosphorus—which is necessary for the growth of FAp into the ambient glass matrix—from the immediate surroundings of FAp crystals.

Another important implication for the growth mechanism arises from the discussion on the role of aluminum in the glass network. If the glass matrix present in sample B (see Table 3) is assumed to be homogeneous, the interaction of AlO_4 tetrahedra and alkali ions is very likely to be such that some part of the total molar fraction of aluminum (those corresponding to the total molar fraction of all alkali ions, i.e., $\sim$ 4.5 mol %) will act as a network former by forming associated groups of AlO_4^- and Na^+/K^+. The aluminum surplus ($\sim$7 mol %) will not be able to find partners for local charge compensation and, consequently, AlO_6 octahedra will occur, known to behave like network modifiers.[27] Thus, a nonbalanced aluminum/alkali ratio (aluminum sur-

plus) results in a decreased viscosity. Transferring these considerations to the occurrence of Al-enriched regions formed at 800 °C has an important consequence. In addition to the (in comparison to 1200 °C) anyway increased viscosity at 800 °C (under the assumption of homogeneously distributed elements in the residual glass), the glass surrounding FAp crystals possesses a further increase in viscosity because of the inhomogeneous aluminum distribution and moreover, according to Table 3, samples C and F, the fluorine content in the residual glass (being significantly lower after 2 min at 800 °C in comparison to that at 1200 °C) further hampers diffusion through the glass. Additionally, the agglomeration of phosphorus apart from apatite growth fronts finally leads to low apatite-crystal growth rates (cf. Figure 5, the FAp crystal diameter is increased by a factor of 1.5 only—even after 5 h of annealing at 800 °C). The latter effect is particularly important since phosphorus diffuses much slower than calcium in the glass matrix.

At 1200 °C, apatite-crystal growth is facilitated because of the following:

(1) There is no phosphorus lack caused by agglomeration processes preceding the crystallization of $AlPO_4$ (the miscibility gap is closed at 1200 °C).[28]

(2) The aluminum distribution is much more homogeneous as compared to that at 800 °C, resulting in combination with the higher fluorine content in the glass in a lower viscosity of the glass near the growth front.

(3) Because of thermal activation, it is much easier to break the linkage between PO_4 groups in the Q^2-type linked matrix glass, which is necessary to enable diffusion of these species toward the crystallization front.

Thus, at 1200 °C, it is much easier for the growing FAp crystal to develop faster moving growth fronts (along the needle axis, presumably by spiral growth) as opposed to slower growing crystal facets perpendicular to it (normal growth).[16]

Needlelike growth of FAp does not occur at 800 °C since, by severely hampered diffusion, the crystal growth following different modes along distinct crystallographic directions is not only superimposed but even outweighed by diffusion control.

(27) ^{27}Al MAS NMR experiments capable of differentiating between 4-fold and 6-fold coordinated aluminium in the residual glass clearly support the model proposed. Since the thorough analysis of those spectra is not straightforward, these results will be published separately.

(28) Moreover, $AlPO_4$ is not a stable crystalline phase at 1200 °C.

4. Conclusions

The results presented here show that the ceramming of multicomponent glasses exhibit exciting effects on one hand, but intense studies are required to elucidate the underlying complex mechanisms on the other hand. In the $SiO_2-Al_2O_3-CaO-P_2O_5-K_2O-F^-$ glass considered here, either needlelike or isometric fluorapatite (FAp) crystals are formed, depending on the thermal treatment.

Upon casting of the glass, some fraction of the liquid−liquid phase separation droplets (PSDs) is directly converted into FAp of the same shape and the remaining droplets are "frozen in". Depending on the temperature of the subsequent heat treatment, more or less of those still amorphous PSDs are dissolved (the higher the temperature, the higher the fraction). Consequently, the resulting residual glass adopts a composition quite different from its starting composition.

At 800 °C, Al- and P-enriched regions are formed between FAp crystals. The inhomogeneous aluminum distribution in combination with a lower fluorine content in the residual glass decreases diffusion coefficients of all elements near FAp crystals. Moreover, the phosphorus supersaturation at the growth front is reduced. Consequently, apatite growth is strongly diffusion controlled at 800 °C and FAp crystals cannot develop the needle shape observed at 1200 °C.

At 1200 °C, enhanced diffusion conditions (due to elevated temperature, homogeneous aluminum distribution, and higher F content in the residual glass) together with the availability of all elements necessary to form FAp enable different growth mechanisms along the needle axis (spiral growth) and perpendicular to it (normal growth) to act. If directional-dependent growth mechanisms are not outweighed by diffusion control, a nonisometric morphology of the apatite crystals can be developed.

Acknowledgment. This work was supported by the Deutsche Forschungsgemeinschaft, Bonn Bad Godesberg, Germany within Contract INK/6. The authors would like to thank Dr. R. Müller, Institut für Physikalische Hochtechnologie, for quenching glass samples. We are indebted to Dr. G. Völksch, Otto-Schott-Institut, FSU Jena, for assistance with SEM-EDXS analyses and Dr. G. Carl, Otto-Schott-Institut, FSU Jena, for stimulating discussions.

CM001203P